Measurement of D2 Dopamine Receptor-Specific Carbon-11-YM-09151-2 Binding in the Canine Brain by PET: Importance of Partial Volume Correction

Jun Hatazawa, Kentaro Hatano, Kiichi Ishiwata, Masatoshi Itoh, Tatsuo Ido, Koichiro Kawashima, Kenichi Meguro, Shoichi Watanuki, and Shinya Seo

Division of Nuclear Medicine, Division of Radiopharmaceutical Chemistry, Cyclotron and Radioisotope Center, Tohoku University, Sendai, Japan

Carbon-11-YM-09151-2 binds highly selectively to D2 dopamine receptors in the brain. Using this ligand, D2 dopamine receptor density (Bmax) and affinity (Kd) in canine striatum were measured. After administering various doses of the ligand in nine experiments, regional uptake was followed by repeated PET scanning for up to 80 min. D2 dopamine receptor specific binding at equilibrium was defined as striatal minus occipital activity after partial volume correction. Bmax and Kd were estimated by Scatchard analysis to be 40.3 pmole/ml of tissue and 22.9 n*M*, respectively. When a low mass dose of the ligand was administered, the bound-to-free ligand ratio in the striatum at equilibrium was consistent with the Bmax/Kd value obtained from the Scatchard analysis. The present study demonstrates the importance of partial volume correction and the Bmax/Kd measurement in a single PET study with carbon-11-YM-09151-2.

J Nucl Med 1991; 32:713–718

YM-09151-2, N-[(2RS,3RS)-1-benzyl-2-methyl-3-pyrrolidinyl]-5-chloro-2-methoxy-4-methylaminobenzamide, is a highly selective antagonist to the D2 dopamine receptor in the brain (*1–2*). We had previously labeled YM-09151-2 with carbon-11 ([^{11}C]YM-09151-2) for a positron-emission tomography (PET) study and demonstrated that [^{11}C]YM-09151-2 is displaced in rat striatum by treatment with sulpride, spiroperidol and YM-09151-2. The D1-dopamine receptor antagonist (SCH-23390) and S2-serotonin receptor antagonist (ritanserin) had no effect on regional distribution of [^{11}C]YM-09151-2 (*3*).

In order to determine D2 dopamine receptor characteristics in the canine brain, we first estimated the volume of striatum in an autopsied brain. Because of the limited spatial resolution of the PET scanner employed, the underestimation of accumulated activity due to the partial volume effect was anticipated (*4*). Bmax and Kd values for the D2 dopamine receptor were determined by administering various mass doses of [^{11}C]YM-09151-2 and applying the Scatchard analysis (*5*) with and without the correction for partial volume effect. In addition, the bound-to-free ligand ratio obtained in the experiment with a low mass dose of [^{11}C]YM-09151-2 was compared with Bmax/Kd value obtained from the Scatchard analysis.

MATERIALS AND METHODS

Animal Preparation

Nine experiments were performed on five male beagles weighing 14–16 kg. Two dogs were studied twice and one dog was studied three times with different administered doses of [^{11}C]YM-09151-2. Dogs were anesthetized with 1%–1.5% of halothane, 2 l/min of N_2O, and 1 l/min of O_2. Catheters were inserted in the femoral artery for monitoring arterial blood pressure and blood sampling and in the femoral vein for administration of [^{11}C]YM-09151-2. A solution of up to 5 ml of the ligand was injected as a bolus. Administered dose and radioactivity levels of [^{11}C]YM-09151-2 in each experiment are summarized in Table 1. Radiochemical purity was more than 99% in all studies. The method of [^{11}C]YM-09151-2 synthesis has been described previously (*3*). The present project was approved by the Research Program Committee of Cyclotron and Radioisotope Center, Tohoku University.

Scan Procedures

A PT-931 model positron emission tomograph (CTI, Knoxville, TN) was employed to measure the regional concentration of the labeled ligand in the brain. This tomograph has a spatial resolution of 8 mm (transaxial) and 7 mm (axial) full-width at half-maximum in the center of the field of view. The scanner has four ring detectors producing seven images simultaneously at 6 mm center to center spacing. The scanning plane was parallel to the line through the external meatus and the inferior orbital

Received Feb. 12, 1990; revision accepted Oct. 1, 1990.

For reprints contact: Jun Hatazawa, MD, PhD, Division of Nuclear Medicine, Cyclotron and Radioisotope Center, Tohoku University, Aramaki-Aoba, Aoba-Ku, Sendai, Japan.

TABLE 1
Summary of Administered Mass Dose and Radioactivity of [^{11}C]YM-09151-2

Experiment no.	Animal no.	Administered mass dose (nmole/kg)	Radioactivity (mCi)	Specific activity (mCi/nmole)
1	1	2.72	13.0	0.299
2	1	8.28	21.0	0.154
3	1	24.30	12.4	0.032
4	2	2.53	6.0	0.147
5	3	0.81	0.5	0.038
6	3	12.50	1.0	0.005
7	4	246.00	5.5	0.001
8	5	6.25	3.0	0.030
9	5	0.10	0.5	0.308

margin. The plane of section was identical to the dog brain atlas described by Lim et al. (*6*). Sequential scanning of 3-min data acquisition started at the time of i.v. administration of [^{11}C]YM-09151-2 and continued for 30 min. Thereafter, 5-min scanning was repeated up to 80 min after administration.

In one of the animals (No. 4), the size of the striatum (caudate nucleus and Putamen) was estimated in an autopsied brain after the PET experiment. Brain sections were also used to relate PET images to brain anatomy and to determine regions of interest (ROIs) for the striatum, occipital cortex, and cerebellum.

Correction for the Partial Volume Effect

To correct the activity accumulated in a small object for the partial volume effect, phantom studies were performed. First, six spherical phantoms with diameters of 30, 20, 15, 12, 10, and 8 mm each were filled with a Na[^{18}F]fluoride solution (3040 nCi/ml). The phantoms were placed in a 20-cm diameter water pool more than 5 cm apart from each other. Spherical phantoms were then filled with water and placed in the Na[^{18}F]fluoride solution (1020 nCi/ml) as a hot background. The center of each sphere was located in the same tomographic plane. Sequential scans were performed for 12 hr in both phantom studies. The phantom images were reconstructed with measured attenuation correction and the Hann filter function used in the animal experiments. All image counts were corrected for physical decay of ^{18}F to the starting time of the first scanning.

A circular ROI with a diameter of 7 mm, which is less than the measured width of the canine striatum, was set on the center of the reconstructed spherical phantom image. Another circular ROI with the same diameter as the phantom diameter was used for pixel count reading. The image counts (cps/pixel) obtained by two different sizes of ROIs were read in each phantom. Assuming that pixel count is fully recovered in the center of the 30-mm "hot" phantom, the ratio of ROI count for each phantom to that for the 30-mm phantom using a 7-mm diameter ROI was defined as the hot spot recovery coefficient (HSRC). For "cold" spherical phantoms, the ratio of the ROI-to-background count was defined as the cold spot recovery coefficient (CSRC).

Estimation of Specific Binding

Tissue time-activity curves for canine striatum, occipital cortex, and cerebellum were obtained after various doses of [^{11}C] YM-09151-2 were administered. Striatal activity was read using a 7-mm diameter ROI and corrected for the partial volume effect according to Kessler et al. (*7*) as follows:

$$\text{Actual Striatal Activity} = (C'_{st} - R_2 * C'_{oc})/R_1,$$

where C'_{st} and C'_{oc} represent the measured activity of striatum and occipital cortex, respectively, and R_1 and R_2 are HSRC and CSRC for a 15-mm diameter spherical phantom estimated by a 7-mm diameter ROI, respectively. Corrected striatal activity minus occipital activity was defined as the specific binding (cps/pixel). This value was divided by the cross calibration factor (cps/pixel/nCi/ml) between the PET scanner and the well counter then divided by the specific activity (mCi/nmole) to obtain a concentration of [^{11}C]YM-09151-2 (pmole/ml tissue). Specific binding in the striatum was also obtained without partial volume correction.

Scatchard Analysis

The peak values of specific binding were determined in each time-activity curve of specific binding. In the present study, total occipital activity at the peak of specific binding was tentatively used as free [^{11}C]YM-09151-2. According to the Scatchard analysis, the bound-to-free ligand ratios were plotted against the bound ligand concentration (pmole/ml tissue). The linear regression lines of seven points before and after correction provided Bmax (x-intercept) and $-1/Kd$ (slope).

Estimation of Bmax/Kd

The time change of concentration of specific binding Cb(t) is expressed as follows (*8,9*):

$$dCb(t)/dt = k_{on} * [Bmax - Cb(t)/SA] * Cf(t) - k_{off} * Cb(t),$$

where Cf(t) denotes the radioactivity levels of free ligand in the reference brain region, the occipital cortex in this study. The bimolecular association rate constant is k_{on}, whereas k_{off} is the unimolecular dissociation rate constant. SA represents specific activity of the ligand.

When specific binding Cb(t) reaches equilibrium, and Cb/SA is negligibly small compared with Bmax, the equation is simplified to:

$$Cb/Cf = Bmax/Kd,$$

where Kd ($= k_{off}/k_{on}$) is the dissociation constant.

In one experiment (No. 9), Cb/SA was 0.40 pmole/ml tissue, which is 1% of Bmax estimated by Scatchard analysis. The ratio Cb/Cf at equilibrium in the experiment was compared with the value of Bmax/Kd obtained from the Scatchard analysis.

HPLC Analysis of Plasma Radioactivity

In experiment No. 1, [^{11}C]YM-09151-2 and its metabolites in arterial plasma were measured by HPLC as described previously (*3*). Radioactivity of the acid-precipitable fraction and peaks d, c, and a+b of the acid-soluble fraction was determined in blood samples taken at 3, 5, 15, and 30 min after injection.

RESULTS

Partial Volume Effect

The measured volumes of the right and left striatum (caudate nucleaus and putamen) were 1.7 ml each in the canine brain. This corresponded to the 15 mm diameter spherical phantom volume (1.77 ml). The maximal length, width, and height were 20, 9, and 15 mm, respectively. The HSCR and CSCR obtained

by using two different ROI were plotted against the phantom diameter in Figure 1. For the 15-mm phantom, the HSCR when 7-mm and 15-mm circular ROIs were used were 75.2% and 47.2%, respectively. The CSCR was 22.0% for a 7-mm diameter ROI and 67.3% for a 15-mm diameter ROI.

D2 Dopamine Receptor-Specific Binding

When 24 nmole/kg (Exp. No. 3) and 246 nmole/kg (Exp. No. 7, demonstrated in Fig. 2) of [^{11}C]YM-09151-2 were administered, no differences in activity distribution were observed among brain structures such as striatum, cerebellum, and cortex. In these two studies as well as in the other seven experiments, no difference in the ligand accumulation between cerebellum and occipital cortex was observed except at the initial phase after administration.

When less than 12.5 nmole/kg of [^{11}C]YM-09151-2 were administered in seven experiments, an elevated accumulation of the ligand in the striatum was observed. Figure 3 illustrates an increased accumulation of [^{11}C]YM-09151-2 to canine striatum when 2.72 nmole/kg of the ligand was administered. Figure 4 showed the partial volume effect corrected specific binding of [^{11}C]YM-09151-2 plotted against time after administration in seven experiments. Specific binding in striatum reached equilibrium within 60 min.

The regression line in the Scatchard analysis was $y=1.760-0.0437x$ ($r=-0.95$, $p<0.01$) as shown in Figure 5. Bmax and Kd were estimated to be 40.3 pmole/ml tissue and 22.9 n*M*, respectively. Without partial volume correction, the regression line was $y=1.178-0.052x$ ($r=-0.94$, $p<0.01$). Bmax and Kd were 22.5 pmole/ml tissue and 19.1 n*M*, respectively.

Estimation of Bmax/Kd

In experiment No. 9, with an administration dose 0.10 nmole/kg, the bound-to-free ratio at equilibrium was 1.78. This value was close to the Bmax/Kd = 1.79 estimated in the Scatchard analysis of seven experiments with different administered mass doses.

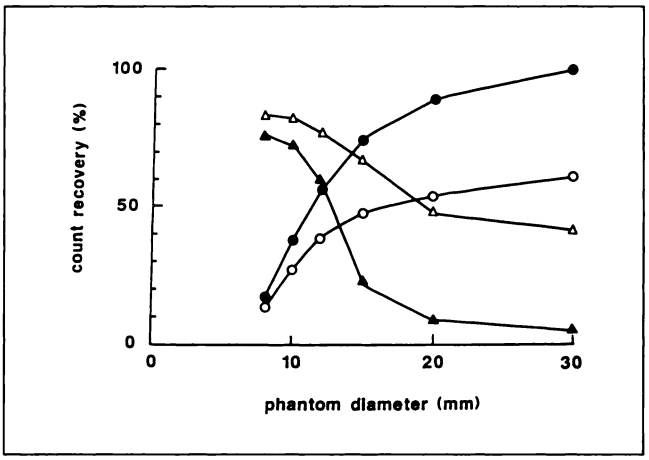

FIGURE 1. Hot spot (● and ○) and cold spot (▲ and △) recovery coefficients as a function of the diameter of a spherical phantom for two different ROIs (● and ▲: 7-mm diameter circular ROI; ○ and △: circular ROI with the same diameter as the phantom). For HSRC, ROI counts were divided by the ROI count obtained from a 30-mm diameter phantom using a 7-mm diameter ROI and the percentage was defined as count recovery. For CSRC, ROI counts read with a 7-mm circle and with the same diameter as the phantom were divided by the background count.

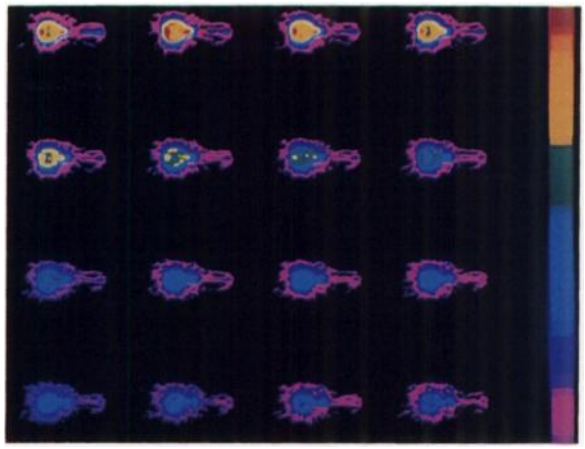

FIGURE 2. Sequential PET images of canine brain obtained after i.v. administration of 246 nmole/kg of [^{11}C]YM-09151-2 are shown from the top left to the bottom right in order of scanning. No difference in uptake of the ligand among brain structures was found, indicating that D2 dopamine receptors were occupied completely by excessive YM-09151-2 and that the non-receptor bound fraction of [^{11}C]YM-09151-2 is distributed uniformly in the brain.

Metabolite Analysis in Plasma

Percentages of the acid-percipitable fraction and peaks d, c, and a+b in the acid-soluble fraction are summarized in Table 2. Only unmetabolized [^{11}C]YM-09151-2 was detected in the acid precipitable fraction. Peaks d, c and a+b were unmetabolized [^{11}C]YM-09151-2, desbenzyl metabolites and unknown metabolites, respectively. Percentages of plasma [^{11}C]YM-09151-2 in the acid-soluble fraction were less than 2% of total activity after 15 min. The ratios of peak d to the total [^{11}C]YM-09151-2 (peak d

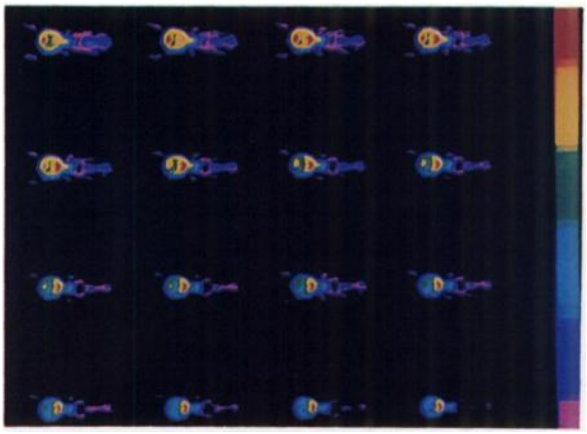

FIGURE 3. Sequential PET images of canine brain scanned after i.v. administration of 2.72 nmole/kg of [^{11}C]YM-09151-2 are shown from the top left to the bottom right in order of scanning. The data acquisition and image reconstruction were identical in the studies in Figure 2 and 3 but the color scale was corrected for radioactivity administered in each study. Elevated accumulation of the ligand in the striatum was clearly visualized in contrast to clearance from the cerebral cortex and cerebellum.

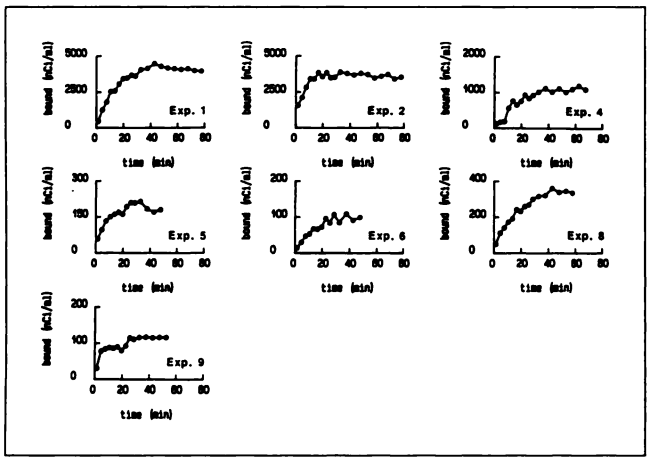

FIGURE 4. Specifically bound [^{11}C]YM-09151-2 to D2 dopamine receptors as a function of time after administration. Striatal activity was first corrected for the partial volume effect then the corrected striatal activity minus occipital was defined as specific binding. Note that specific binding reached equilibrium within 60 min after injection in all experiments.

+ acid precipitable fraction) in plasma were 12.6, 4.7, 3.6 and 5.1% at 3, 15, 30, and 60 min, respectively.

DISCUSSION

Since dopamine receptor-specific binding of a neuroleptic drug in human brain was visualized using [^{11}C]N-methyl-spiperone by Wagner et al. (*10*), a number of analytical methods have been developed to measure in vivo receptor characteristics quantitatively using PET (*8, 9, 11–16*). In any method, the first step for quantitation should be to accurately measure the activity of ligand specifically bound to receptors. However, because of the limited spatial resolution of our present PET scanner, radioactivity accumulation in small objects such as canine striatum may be underestimated due to the partial volume

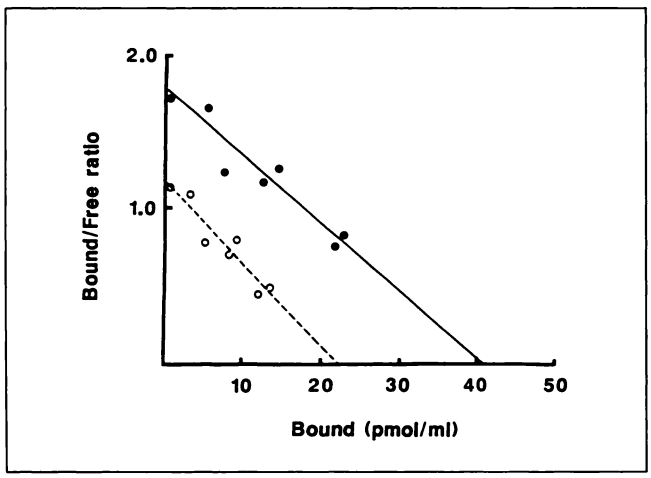

FIGURE 5. Scatchard plots of seven experiments with different administered doses of [^{11}C]YM-09151-2. Closed circles indicate points after correction for the partial volume effect and open circles indicate points before correction.

TABLE 2
Metabolites of [^{11}C]YM-09151-2 in Plasma After Intravenous Injection

Time (min)	Acid-precipitable radioactivity (%)	Acid-soluble radioactivity		
		peak d (%)	peak c (%)	peak a + b (%)
3	51.4	7.4	18.6	22.6
15	34.7	1.7	12.8	50.8
30	40.3	1.5	5.4	52.8
60	35.3	1.9	4.3	58.5

effect (*4*). For example, the radioactivity accumulated in primate striatum measured by means of PET was half of that in samples dissected postmortem and measured with a well counter (*17*). Before applying any kinetic model to PET measurements in animal experiments or even in human studies when atrophic change of striatum is anticipated, the partial volume effect of the PET scanner employed should be first examined.

In kinetic measurements, partial volume correction should be accurately performed in all images measured, where the striatum-to-background ratio may change during scanning and differ between blocked and unblocked studies. Wong et al. (*11*) performed this correction by making the recovery coefficient a function of time. We, however, used a single value of HSRC and CSRC throughout the experiments, because only the specifically bound activity and bound-to-free activity ratios at "steady-state" were required in the present analysis.

D2 dopamine receptor-specific binding can be defined as the ratioactivity in striatum reduced with that in any reference regions, typically the cerebellum. This estimation assumes that the free and non-specifically bound ligand and ^{11}C-labeled metabolites in striatum are the same as that in the reference region. When more than 24 nmole/kg of [^{11}C]YM-09151-2 were administered, no significant difference in ligand activity was seen in the striatum, cerebellum, and cortical region. This implies that striatal D2 dopamine receptors were occupied by the excess YM-09151-2 and that the total fraction of free and nonspecifically bound [^{11}C]YM-09151-2 in addition to ^{11}C-labeled metabolites may be at the same levels among these brain structures. This validated the measurement of receptor bound fraction by subtracting occipital or cerebellar activity from total striatal activity in the case of [^{11}C]YM-09151-2.

Instead of the cerebellum, the occipital cortex, where few D2 dopamine receptors were distributed (*18*), was defined as the reference region, since in previous rat studies we found unbound but YM-09151-2 specific binding sites in the cerebellum (*3*). However, in canine brain, there was no significant difference in the accumulation between the occipital cortex and the cerebellum even after administration of excess doses. Therefore, both the occipital cortex and cerebellum were possible reference regions in canine brain.

The levels of free, nonspecifically bound ligand, and metabolites are unknown in canine brain. This uncertainty is a possible error source for quantitation. The concentration of free ligand in the reference region can be calculated according to Logan et al. when the free ligand fraction in plasma is measured (*15*). They described $f_1/f_2=k_1/k_2$, where f_1 and f_2 denote the free fraction of the ligand in plasma and tissue, respectively, and k_1 and k_2 represented transport rates from plasma to tissue and from tissue back to plasma, respectively. Assuming that no metabolites pass into brain, k_1 and k_2 were determined by the best fit in a least-squares sense from occipital or cerebellar activity data. In experimental No. 1, the measured k_1 and k_2 in occipital cortex was 0.723 and 0.165, respectively. Free fraction in plasma f_1 was found to be 0.045 in HPLC analysis (mean value of samples taken at 15, 30, and 60 min). From these values, f_2 was estimated to be on the order of 1% for [^{11}C]YM-09151-2.

When the Scatchard analysis is applied to PET measurements, specific binding equilibrium should be reached within a short time. Farde et al. reported that specific binding of [^{11}C]raclopride, another substituted benzamide, occurred within 30 min in human striatum (*14*). The steady-state of specific binding of [^{11}C]YM-09151-2 occurred at 40–60 min after injection, later than that of [^{11}C]-raclopride, but continued longer (*19*).

Bmax and Kd after correction for the partial volume effect were 1.8- and 1.2-fold higher than before the correction, respectively. In the present study, the Bmax value after correction was much closer to 36 pmole/ml, the value measured in the in vitro study by Niznik et al. using [^{3}H]YM-09151-2 (*2*). They also estimated the Kd in canine striatal membrane to be 0.057 n*M* in the presence of 120 m*M* sodium chloride and 0.32 n*M* in the absence of sodium chloride. When we set the fraction of free ligand to 0.01 as calculated above, instead of an assumed value of 1 (total occipital activity as free fraction), the Kd of 22.9 n*M* may be reduced to 0.229 n*M*, which is much closer to the in vitro estimates.

The bound-to-free ligand ratio at equilibrium obtained by a single PET study with a low mass dose was consistent with Bmax/Kd determined by Scatchard analysis. In order to estimate Bmax and Kd separately, a concurrent study is required with a larger mass dose which may occupy a significant number of D2 receptors and may induce pharmacologic effect. A possible alternative method for measuring Bmax and Kd is kinetic analysis as described by Farde et al. (*14*). This method depends upon high radioactivity levels of [^{11}C]YM-09151-2 for measuring plasma metabolites with HPLC and a low mass dose for solving the model equation which contains a non-linear term when Cb/SA is not negligibly small compared with Bmax. Although we measured plasma metabolites in experiment No. 1, Cb/SA was 35% of Bmax and kinetic analysis could not be applied in this case.

In conclusion, the present study demonstrated the importance of correction for the partial volume effect when small structures are scanned. We validated the Bmax/Kd measurement by measuring the bound-to-free ligand ratio at equilibrium in a single PET study in which a low mass dose of [^{11}C]YM-09151-2 was administered.

ACKNOWLEDGMENT

The authors thank the members of the Cyclotron RI Center, Tohoku University. We also thank Dr. I. Kanno of the Research Center of Brain and Blood Vessels, Akita, Japan; Drs. O. Inoue and H. Fukuda of the Research Institute of Radiation Science, Chiba, Japan; and Dr. K. Yanai of The First Department of Pharmacology, Tohoku University School of Medicine for their valuable comments. The authors are grateful to Yamanouchi Pharmaceutical Co., Ltd., for supplying YM-09151-2. We also thank Miss Y. Shibuya for preparing the manuscript.

The present work was supported by grant-in-aid No. 61870047 (TI). One of the authors (JH) was supported by grants 63770765 and 01770776 of the Ministry of Education, Japan.

REFERENCES

1. Terai M, Usuda S, Kuroiwa I, et al. Selective binding of YM-09151-2, a new potent neuroleptic, to D_2 dopaminergic receptors. *Jpn J Pharmacol* 1983;33:749–755.
2. Nikzik HB, Grigoriadis DE, Pri-Bar I, et al. Dopamine D_2 receptors selectively labeled by a benzamide neuroleptic:[^{3}H]ym-09151-2. *Arch Pharmacol* 1985;329:333–343.
3. Hatano K, Ishiwata K, Kawashima K, et al. D_2-dopamine receptor specific brain uptake of carbon-11-labeled YM-09151-2. *J Nucl Med* 1989;30:515–522.
4. Hoffman EJ, Huang SC, Plummer D, Phelps ME. Quantitation in positron emission computed tomography. 1. Effect of object size. *J Comput Assist Tomogr* 1979;3:299–308.
5. Scatchard G. The attractions for small molecules and ions. *Ann NY Acad Sci* 1949;51:660–672.
6. Lim RKS, Liu CN, Moffitt RL. *A stereotaxic atlas of the dog's brain.* Springfield, IL: Charles C. Thomas; 1960.
7. Kessler RM, Ellis JR Jr, Eden M. Analysis of emission tomographic scan data: limitations imposed by resolution and background. *J Comput Assist Tomogr* 1984;3:514–522.
8. Mintun MA, Raichle ME, Kilbourn MR, Wooten GF, Welch MJ. A quantitative model for the in vivo assessment of drug binding sites with positron emission tomography. *Ann Neurol* 1984;15:217–227.
9. Wong DF, Gjedde A, Wagner HN Jr. Quantification of neuroreceptors in the living human brain. I. Irreversible binding of ligands. *J Cereb Blood Flow Metab* 1986;6:137–146.
10. Wagner HN Jr., Burns HD, Dannals RF, et al. Imaging dopamine receptors in human brain by positron emission tomography. *Science* 1983;221:1264–1266.
11. Wong DF, Gjedde A, Wagner HN Jr, et al. Quantification of neuroreceptors in the living human brain. II. Inhibition studies of receptor density and affinity. *J Cereb Blood Flow Metab* 1986;6:147–153.
12. Perlmutter JS, Larson KB, Raichle ME, et al. Strategies for in vivo measurement of receptor binding using positron emission tomography. *J Cereb Blood Flow Metab* 1986;6:154–169.
13. Farde L, Hall H, Ehrin E, et al. Quantitative analysis of D2 dopamine receptor binding in the living human brain by PET. *Science* 1986;231:258–261.
14. Farde L, Eriksson L, Blomquist G, Halldin C. Kinetic analysis of central [^{11}C]raclopride binding to D2-dopamine receptors studied by PET-a comparison to the equilibrium analysis. *J Cereb Blood Flow Metab* 1989;9:696–709.
15. Logan J, Wolf AP, Shiue CY, Fowler JS. Kinetic modeling of receptor-ligand binding applied to positron emission tomographic studies with neuroleptic tracers. *J Neurochemistry* 1987;48:73–83.
16. Huang SC, Bahn MM, Barrio JR, et al. A double-injection technique for in vivo measurement of dopamine D_2-receptor density in monkeys with 3-(2'-[^{18}F]fluoroethyl)spiperone and dynamic positron emission tomography.

J Cereb Blood Flow Metab 1989;9:850–858.
17. Eckernas SA, Aquilonius SM, Hartvig P, et al. Positron emission tomography (PET) in the study of dopamine receptors in the primate brain: evaluation of a kinetic model using ^{11}C-N-methyl-spiperone. *Acta Neurol Scand* 1987;75:168–178.
18. Lidow MS, Goldman-Rakic PS, Rakic P, Innis RB. Dopamine D2 receptors in the cerebral cortex: distribution and pharmacological characterization with [^{3}H]raclopride. *Proc Natl Acad Sci USA* 1989;86:6412–6416.
19. Hartvig P, Eckernas SA, Ekblom B, et al. Receptor binding and selectivity of three ^{11}C-labeled dopamine receptor antagonists in the brain of rhesus monkeys studied with positron emission tomography. *Acta Neurol Scand* 1988;77:314–321.

SELF-STUDY TEST
Gastrointestinal Nuclear Medicine
ANSWERS

(continued from p. 685)

ITEM 1: Pediatric Gastric Emptying

ANSWER: D

The time-activity curve (Fig. 1) shows a normal initial emptying pattern of the stomach. Later, however, the stomach appears to refill. This is a common artifact due to overlapping of small bowel within the gastric region of interest. Superimposition of activity in loops of small bowel is a major problem encountered in quantitative evaluation of gastrointestinal scintigraphy. It is frequently observed in studies of enterogastric reflux, small bowel transit, and gastric emptying. Some investigators state it is not a significant problem, but anyone who has analyzed enough gastrointestinal studies recognizes it frequently. Superimposition can be recognized easily by reviewing the images and regions of interest. As Seibert et al. point out, overlap of small bowel activity with that in the stomach is a particular problem in children. Repositioning can be used to swing the stomach and duodenum away from each other.

Reference

1. Seibert JJ, Byrne WJ, Euler AR. Gastric emptying in children: unusual patterns detected by scintigraphy. *AJR* 1983;141:49–51.

ITEM 2: Protein-Losing Enteropathy

Answer: B

The ^{51}Cr-albumin study demonstrates abnormally increased fecal excretion of the radiolabeled protein. Therapy for excessive gastrointestinal protein loss depends on proper identification of the underlying disorder. Small bowel diseases, including tropical sprue, Whipple's disease, and bacterial or parasitic enteritis, are treatable with antimicrobial drugs and occasionally may show some response to steroids. A normal small bowel biopsy in this case would effectively eliminate these diseases as a cause of this patient's protein-losing enteropathy. The majority of patients with adult celiac disease (sprue) will respond to an adequate gluten-free diet. No other condition will respond so dramatically. The nonspecific findings of the barium study, however, do not indicate primary small intestinal disease in this patient. Hypoproteinemia due to protein-losing enteropathy has been described in patients with congestive heart failure, but is especially common in patients with constrictive pericarditis. Prior to the advent of antituberculous drugs, tuberculosis was the most common cause of constrictive pericarditis. The left ventricular ejection fraction may be normal because it reflects left ventricular systolic function. Heart size also may be normal. Because of the past history of tuberculosis, the most likely cause of protein-losing enteropathy in this case is constrictive pericarditis. Diastolic expansion of both ventricles is affected in constrictive pericarditis; therefore, cardiac catheterization will show elevated pressures in all four chambers. Both the right and left ventricular pressure curves will show the "square-root sign" with a rapid early diastolic dip and then a high diastolic plateau. This is the characteristic hemodynamic sign of constrictive pericarditis.

ITEM 3: Scintigraphy of Hepatoblastoma

Answer: E

The anterior ^{99m}Tc-sulfur colloid image (Fig. 2A) shows a large mass replacing the majority of the right lobe of the liver. There is increased blood-pool activity of the lesion in the right lobe compared with the uninvolved left lobe of the liver, seen in the ^{99m}Tc-red blood cell study (Fig. 2B). The activity does not approach that of the cardiac blood-pool. In addition, within the hypervascular mass are areas of reduced activity, probably indicating focal necrosis. The ^{99m}Tc-disofenin study (Fig. 2C) shows marked inhomogeneity of tracer uptake in the dominant mass. This indicates small islands of preserved hepatic parenchyma within the mass. The upper edge of the gallbladder is stretched but excretion of the tracer into the gastrointestinal tract excludes biliary obstruction.

Cavernous hemangiomas may present as solitary or multiple lesions within the liver, whereas hemangioendotheliomas are usually multifocal. Radionuclide angiography may reveal increased perfusion. If there is an enlarged blood pool, however, slow transit through such tumors may suggest a hypovascular lesion. Blood-pool imaging with labeled red blood cells confirms the vascularity of these lesions with intensity typically approaching that of the cardiac blood pool. Studies performed with hepatobiliary agents will show focal defects in the early images and these do not fill in with time because the tumors do not contain functioning hepatocytes. The blood-pool image in this case shows only slightly increased activity, making a diagnosis of cavernous hemangioma unlikely.

Focal nodular hyperplasia is rare in children. The lesions in the liver may be single or multiple, and these may exhibit either decreased, normal, or increased uptake of ^{99m}Tc-sulfur colloid. The perfusion may be normal or increased. Labeled red blood cell imaging tends to be normal, with lesion intensity equaling that of the normal hepatic parenchyma. Most lesions of focal nodular hyperplasia will show uptake of iminodiacetic acid derivatives with intensity equal to that of the surrounding liver. In some instances, however, these lesions may have relatively few hepatocytes, and a persistent defect is noted. In this case, the single defect, with slightly increased blood-pool activity and no evidence of ^{99m}Tc-disofenin accumulation, argues against focal nodular hyperplasia (as does the rarity of this disorder in children).

Congenital biliary ductal ectasia is an abnormality characterized by segmental, saccular dilatation of the intrahepatic bile ducts in the absence of obstruction. Two forms are recognized. The first (also known as Caroli's disease) is associated with bile stasis, cholangitis, intrahepatic calculus formation, and renal tubular ectasia. The second form is characterized by congenital hepatic fibrosis, cirrhosis, and portal hypertension. Images with ^{99m}Tc-sulfur colloid will show defects due to ductal enlargement and changes of cirrhosis may be present. With labeled red blood cell imaging, the lesions will not show increased vascularity. There will be delayed filling and retention of tracer in the enlarged ducts on hepatobiliary imaging. This patient clearly does not have congenital biliary ductal ectasia.

Neuroblastoma metastasizing to the liver tends to show multiple lesions by ^{99m}Tc-sulfur colloid imaging. Perfusion to the areas of involvement is decreased during the angiographic phase. Red blood cell scintigraphy reveals normal or decreased activity. Iminodiacetic acid imaging reveals focal "cold" lesions, which do not fill in with time. Although neuroblastoma cannot be definitely excluded, the single lesion in this patient with somewhat increased blood-pool activity suggests a hepatoblastoma, rather than metastatic neuroblastoma.

Hepatoblastoma usually presents as a single lesion in the liver. As with most malignant processes, the lesions appear hypovascular during the angiographic phase, although early blood flow may be seen within the tumor consistent with arterialization. Blood-pool imaging with labeled red blood cells shows a slight increase in vascularity, although the intensity is less than that of the heart. As with most malignant lesions (except some cases of differentiated hepatoma), hepatobiliary imaging with iminodiacetic acid derivatives shows a persistent defect in the liver.

Demonstration of a solitary lesion with sulfur colloid imaging is not specific. In general, added specificity can result from complementary evaluation by ultrasonography or computed tomography. The addition of further scintigraphic studies, such as labeled red blood cell and hepatocyte imaging, do add some specificity as well. The scintigraphic findings

(continued on p. 728)